



CHORUS

This is the accepted manuscript made available via CHORUS. The article has been published as:

Fermi arc electronic structure and Chern numbers in the type-II Weyl semimetal candidate $\text{Mo}_x\text{W}_{1-x}\text{Te}_2$

Ilya Belopolski *et al.*

Phys. Rev. B **94**, 085127 — Published 15 August 2016

DOI: [10.1103/PhysRevB.94.085127](https://doi.org/10.1103/PhysRevB.94.085127)

Electronic structure and Chern numbers in the Type II Weyl semimetal candidate $\text{Mo}_x\text{W}_{1-x}\text{Te}_2$

Ilya Belopolski^{*,1,†}, Su-Yang Xu^{*,1}, Yukiaki Ishida^{*,2}, Xingchen Pan^{*,3}, Peng Yu^{*,4}, Daniel S. Sanchez¹, Hao Zheng¹, Madhab Neupane⁵, Nasser Alidoust¹, Guoqing Chang^{6,7}, Tay-Rong Chang⁸, Yun Wu⁹, Guang Bian¹, Shin-Ming Huang^{6,7,10}, Chi-Cheng Lee^{6,7}, Daixiang Mou⁹, Lunan Huang⁹, You Song¹¹, Baigeng Wang³, Guanghou Wang³, Yao-Wen Yeh¹², Nan Yao¹², Julien E. Rault¹³, Patrick Le Fèvre¹³, François Bertran¹³, Horng-Tay Jeng^{8,14}, Takeshi Kondo², Adam Kaminski⁹, Hsin Lin^{6,7}, Zheng Liu^{4,15,16,‡}, Fengqi Song^{3,§}, Shik Shin² and M. Zahid Hasan^{1,12,¶}

¹Laboratory for Topological Quantum Matter and Spectroscopy (B7),
Department of Physics, Princeton University, Princeton, New Jersey 08544, USA

²The Institute for Solid State Physics (ISSP), University of Tokyo,
Kashiwa-no-ha, Kashiwa, Chiba 277-8581, Japan

³National Laboratory of Solid State Microstructures,
Collaborative Innovation Center of Advanced Microstructures,
and Department of Physics, Nanjing University, Nanjing, 210093, P. R. China

⁴Centre for Programmable Materials, School of Materials Science and Engineering,
Nanyang Technological University, 639798, Singapore

⁵Department of Physics, University of Central Florida, Orlando, FL 32816, USA

⁶Centre for Advanced 2D Materials and Graphene Research Centre,
National University of Singapore, 6 Science Drive 2, 117546, Singapore

⁷Department of Physics, National University of Singapore, 2 Science Drive 3, 117546, Singapore

⁸Department of Physics, National Tsing Hua University, Hsinchu 30013, Taiwan

⁹Ames Laboratory, U.S. DOE and Department of Physics and Astronomy, Iowa State University, Ames, Iowa 50011, USA

¹⁰Department of Physics, National Sun Yat-sen University, Kaohsiung 80424, Taiwan

¹¹State Key Laboratory of Coordination Chemistry, School of Chemistry and Chemical Engineering,
Collaborative Innovation Center of Advanced Microstructures,
Nanjing University, Nanjing, 210093, P. R. China

¹²Princeton Institute for Science and Technology of Materials,
Princeton University, Princeton, New Jersey, 08544, USA

¹³Synchrotron SOLEIL, L'Orme des Merisiers, Saint-Aubin-BP 48, 91192 Gif-sur-Yvette, France

¹⁴Institute of Physics, Academia Sinica, Taipei 11529, Taiwan

¹⁵NOVITAS, Nanoelectronics Centre of Excellence, School of Electrical and Electronic Engineering,
Nanyang Technological University, 639798, Singapore

¹⁶CINTRA CNRS/NTU/THALES, UMI 3288, Research Techno Plaza,
50 Nanyang Drive, Border X Block, Level 6, 637553, Singapore

(Dated: July 17, 2016)

It has recently been proposed that electronic band structures in crystals can give rise to a previously overlooked type of Weyl fermion, which violates Lorentz invariance and, consequently, is forbidden in particle physics. It was further predicted that $\text{Mo}_x\text{W}_{1-x}\text{Te}_2$ may realize such a Type II Weyl fermion. Here, we first show theoretically that it is crucial to access the band structure above the Fermi level, ε_F , to show a Weyl semimetal in $\text{Mo}_x\text{W}_{1-x}\text{Te}_2$. Then, we study $\text{Mo}_x\text{W}_{1-x}\text{Te}_2$ by pump-probe ARPES and we directly access the band structure > 0.2 eV above ε_F in experiment. By comparing our results with *ab initio* calculations, we conclude that we directly observe the surface state containing the topological Fermi arc. We propose that a future study of $\text{Mo}_x\text{W}_{1-x}\text{Te}_2$ by pump-probe ARPES may directly pinpoint the Fermi arc. Our work sets the stage for the experimental discovery of the first Type II Weyl semimetal in $\text{Mo}_x\text{W}_{1-x}\text{Te}_2$.

Weyl fermions have been known since the early twentieth century as chiral particles associated with solutions to the Dirac equation at zero mass^{1,2}. In particle physics, imposing Lorentz invariance uniquely fixes the dispersion for a Weyl fermion. However, effective field theories in condensed matter physics are not required to obey Lorentz invariance, leaving a freedom in the Weyl fermion dispersion. Recently, it was dis-

covered that this freedom allows a new type of Weyl fermion to arise in a crystalline band structure, distinct from the Weyl fermion relevant to particle physics³⁻⁹. This Type II Weyl fermion strongly violates Lorentz invariance and has a dispersion characterized by a Weyl cone which is tilted over on its side. It was further predicted that a Type II Weyl semimetal arises in WTe_2 ³. Concurrently, MoTe_2 and $\text{Mo}_x\text{W}_{1-x}\text{Te}_2$ were predicted to be Weyl semimetals¹⁰⁻¹² and, more recently, several additional Type II Weyl semimetal candidates have been proposed¹³⁻¹⁵. All theoretical studies found that all Weyl points in the $\text{Mo}_x\text{W}_{1-x}\text{Te}_2$ series are above

*These authors contributed equally to this work.

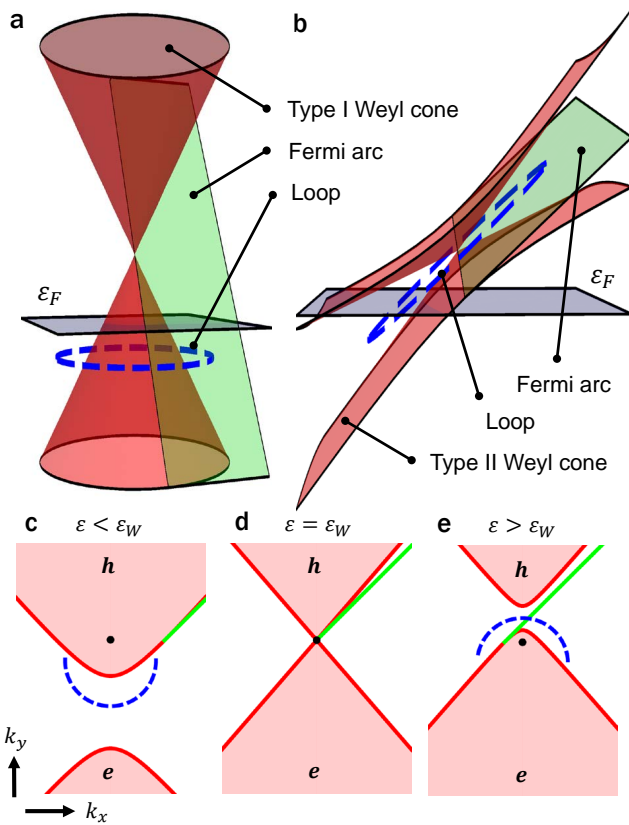


FIG. 1: **Chern numbers in Type II Weyl semimetals.** A loop (dashed blue line) to show a nonzero Chern number in (a) a Type I Weyl cone and (b) a Type II Weyl cone. Suppose the Weyl point lies above ϵ_F . In the simplest case, it is clear that for a Type I Weyl cone, we can show a nonzero Chern number by counting crossings of surface states on a closed loop which lies entirely below the Fermi level. This is not true for a Type II Weyl semimetal. (c-e) Constant-energy cuts of (b). We can attempt to draw a loop below ϵ_F , as in (c), but we find that the loop runs into the bulk hole pocket. We can close the loop by going to $\epsilon > \epsilon_W$, as in (e). However, then the loop must extend above ϵ_F .

the Fermi level, ϵ_F . While angle-resolved photoemission spectroscopy (ARPES) would be the technique of choice to directly demonstrate a Type II Weyl semimetal in $\text{Mo}_x\text{W}_{1-x}\text{Te}_2$, conventional ARPES can only study occupied electron states, below ϵ_F , making it challenging to access the Weyl semimetal state in $\text{Mo}_x\text{W}_{1-x}\text{Te}_2$. Nonetheless, several ARPES works attempt to access the Weyl semimetal state in MoTe_2 and WTe_2 by studying the band structure above ϵ_F in the tail of the Fermi-Dirac distribution^{16–18}, while other works have tried to demonstrate a Type II Weyl semimetal in MoTe_2 and WTe_2 in ARPES by studying only the band structure below ϵ_F ^{19–23}. We note also a recent experimental study of Type II Weyl fermions in an unrelated compound^{24,25}.

Here, we first argue that it's crucial to study the band structure above ϵ_F to show a Weyl semimetal in $\text{Mo}_x\text{W}_{1-x}\text{Te}_2$, even if the Fermi arcs fall partly below

the Fermi level. Next, we experimentally demonstrate that we can access states sufficiently far above ϵ_F using a state-of-the-art photoemission technique known as pump-probe ARPES. We find excellent agreement between our pump-probe ARPES data and *ab initio* calculations, suggesting that $\text{Mo}_x\text{W}_{1-x}\text{Te}_2$ is a Type II Weyl semimetal. We suggest that a future pump-probe ARPES study may directly pinpoint the topological Fermi arc. In this way, our results set the theoretical and experimental groundwork for demonstrating the first Type II Weyl semimetal in $\text{Mo}_x\text{W}_{1-x}\text{Te}_2$. Our work also opens the way to studying the unoccupied band structure and time-relaxation dynamics of transition metal dichalcogenides by pump-probe ARPES.

Can we show that a material is a Weyl semimetal if the Weyl points are above the Fermi level, $\epsilon_W > \epsilon_F$? For the simple case of a well-separated Type I Weyl point of chiral charge ± 1 , it is easy to see that this is true. Specifically, although we cannot see the Weyl point itself, the Fermi arc extends below the Fermi level, see Fig. 1(a). Therefore, we can consider a closed loop in the surface Brillouin zone which encloses the Weyl point. By counting the number of surface state crossings on this loop we can demonstrate a nonzero Chern number²⁶. In our example, we expect one crossing along the loop. By contrast, this approach fails for a well-separated Type II Weyl point above ϵ_F . In particular, recall that when counting Chern numbers, the loop we choose must stay always in the bulk band gap. As a result, for the Type II case we cannot choose the same loop as in the Type I case since the loop would run into the bulk pocket. We might instead choose a loop which is slanted in energy, see Fig. 1(b), but such a loop would necessarily extend above ϵ_F . Alternatively, we can consider different constant energy cuts of the Type II Weyl cone. In Figs. 1(c-e), we show constant-energy cuts of the Type II Weyl cone and Fermi arc. We see that we cannot choose a closed loop around the Weyl point by looking only at one energy, because the loop runs into a bulk pocket. However, we can build up a closed loop from segments at energies above and below the Weyl point, as in Figs. 1(c,e). But again, we must necessarily include a segment on a cut at $\epsilon > \epsilon_W$. We find that for a Type II Weyl semimetal, if the Weyl points are above the Fermi level, we must study the unoccupied band structure.

Next, we argue that in the specific case of $\text{Mo}_x\text{W}_{1-x}\text{Te}_2$ we must access the unoccupied band structure to show a Weyl semimetal. In the Supplemental Material, we present a detailed discussion of the band structure of $\text{Mo}_x\text{W}_{1-x}\text{Te}_2$ ²⁷. Here, we only note a key result, consistent among all *ab initio* calculations of $\text{Mo}_x\text{W}_{1-x}\text{Te}_2$, that all Weyl points are Type II and are above the Fermi level^{3,10–12}. These facts are essentially sufficient to require that we access the unoccupied band structure. However, it is useful to provide a few more details. Suppose that the Fermi level of $\text{Mo}_x\text{W}_{1-x}\text{Te}_2$ roughly corresponds to the case of Fig. 1(c). To count a Chern number using only the band structure below the

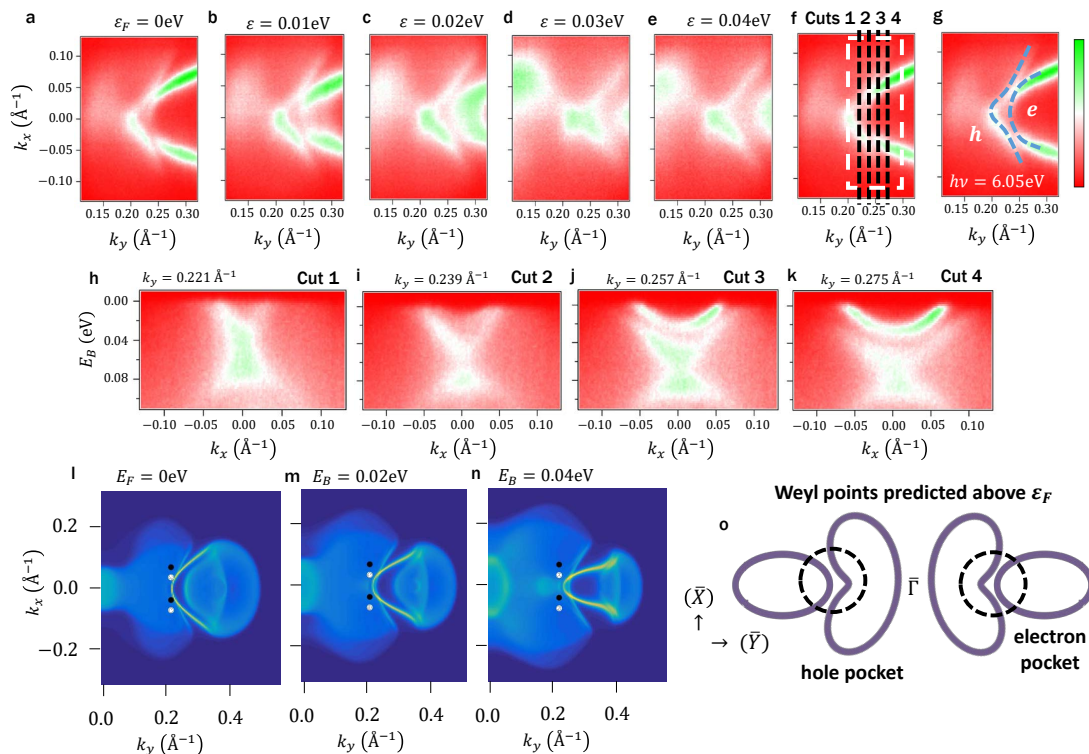


FIG. 2: $\text{Mo}_{0.45}\text{W}_{0.55}\text{Te}_2$ below the Fermi level. (a-g) Conventional ARPES spectra of the constant-energy contour. We observe a palmier-shaped hole pocket and an almond-shaped electron pocket. The two pockets approach each other and we directly observe a beautiful avoided crossing near ε_F where they hybridize, in (a). This hybridization is expected to give rise to Weyl points above ε_F . (h-k) ARPES measured $E_B - k_y$ dispersion maps along the cuts shown in (f). We expect Weyl points or Fermi arcs above the Fermi level at certain k_y where the pockets approach. (l-n) Constant-energy contours for $\text{Mo}_{0.4}\text{W}_{0.6}\text{Te}_2$ from *ab initio* calculations. The black and white dots indicate the Weyl points, above ε_F . Note the excellent overall agreement with the ARPES spectra. The offset on the k_y scale on the ARPES spectra is set by comparison with calculation. (o) Cartoon of the palmier and almond at the Fermi level. Based on calculation, we expect Weyl points above ε_F where the pockets intersect.

Fermi level, we need to find a path enclosing a nonzero chiral charge while avoiding the bulk hole and electron pockets. We can try to trace a path around the entire hole pocket. However, as we will see in Fig. 2, the Weyl point projections all fall in one large hole pocket at ε_F . As a result, tracing around the entire hole pocket encloses zero chiral charge, see also an excellent related discussion in Ref.²⁸. Therefore, demonstrating a Weyl semimetal in $\text{Mo}_x\text{W}_{1-x}\text{Te}_2$ requires accessing the unoccupied band structure.

We briefly introduce the occupied band structure of $\text{Mo}_x\text{W}_{1-x}\text{Te}_2$. We present ARPES spectra of $\text{Mo}_{0.45}\text{W}_{0.55}\text{Te}_2$ below the Fermi level, see Figs. 2(a-k). We observe a palmier-shaped hole pocket and an almond-shaped electron pocket which chase each other as we scan in binding energy. We find excellent agreement between our ARPES results and *ab initio* calculation, see Fig. 2(l-n). Based on calculation, at two energies above ε_F , the pockets catch up to each other and intersect, forming two sets of Weyl points W_1 and W_2 , see Fig. 2(o) and also the Supplemental Material²⁷.

Next, we show that we can directly access the relevant unoccupied states in $\text{Mo}_x\text{W}_{1-x}\text{Te}_2$ with pump-

probe ARPES. In our experiment, we use a 1.48eV pump laser to excite electrons into low-lying states above the Fermi level and a 5.92eV probe laser to perform photoemission²⁹. We first study $\text{Mo}_{0.45}\text{W}_{0.55}\text{Te}_2$ along $\bar{\Gamma} - \bar{Y}$ at fixed $k_x = 0\text{\AA}^{-1}$, see Figs. 3(a,b). The sample responds beautifully to the pump laser and we observe a dramatic evolution of the bands up to energies $> 0.2\text{eV}$ above ε_F . We find, similarly that we can directly access the unoccupied band structure on a cut at fixed $k_y \sim k_W$, see Figs. 3(c,d). Further, by plotting constant-energy cuts, we can directly observe that the almond pocket continues to grow above ε_F , while the palmier pocket recedes, consistent with calculation, see Figs. 3(e-j). We note that all available calculations of $\text{Mo}_x\text{W}_{1-x}\text{Te}_2$ place the Weyl points $< 0.1\text{eV}$ above the Fermi level. In addition, the Weyl point projections are all predicted to lie within 0.25\AA^{-1} of the $\bar{\Gamma}$ point^{3,10-12}. We see that our pump-probe measurement easily accesses the relevant region of reciprocal space to show a Weyl semimetal in $\text{Mo}_x\text{W}_{1-x}\text{Te}_2$ for all x .

We next present evidence for a Weyl semimetal in $\text{Mo}_{0.45}\text{W}_{0.55}\text{Te}_2$. The agreement between our pump-probe ARPES spectra and *ab initio* calculation strongly

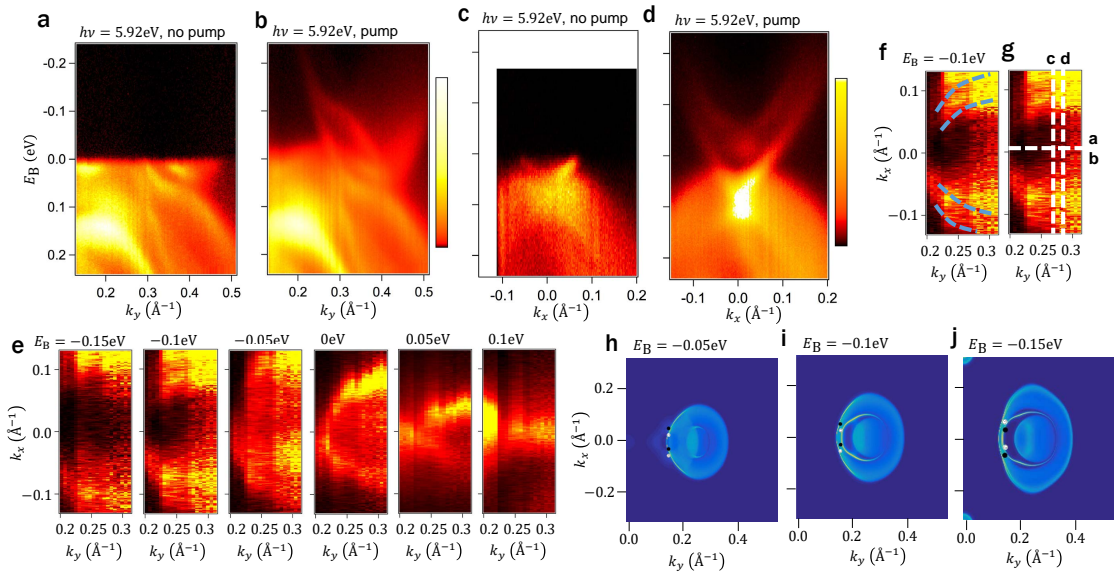


FIG. 3: **Mo_{0.45}W_{0.55}Te₂ above the Fermi level.** (a,b) $E_B - k_y$ dispersion maps of Mo_{0.45}W_{0.55}Te₂ along the $\bar{\Gamma} - \bar{Y}$ direction at $k_x = 0$ with and without the pump laser. The sample responds beautifully to the pump laser, allowing us access to the band structure $> 0.2\text{eV}$ above ε_F , well above the predicted energies of the Weyl points. (c,d) Dispersion maps of Mo_{0.45}W_{0.55}Te₂ with and without pump on a cut parallel to $\bar{\Gamma} - \bar{X}$ at (c) $k_y \sim 0.29\text{\AA}^{-1}$ and (d) $k_y \sim 0.26\text{\AA}^{-1}$. (e-g) The evolution of the almond pocket in energy. We observe that the almond pocket evolves into two nested contours, seen most clearly at $E_B = -0.1\text{eV}$. (h-j) Calculation of the Fermi surface for Mo_{0.4}W_{0.6}Te₂ above ε_F . We see two nested electron pockets, consistent with the measured Fermi surface at $E_B = -0.1\text{eV}$.

suggests that Mo_{0.45}W_{0.55}Te₂ is a Weyl semimetal. We consider the spectrum at fixed $k_y \sim k_W$, see Figs. 4(a-d). We find an upper electron pocket (1) with a short additional surface state (2), a lower electron pocket (3) and the approach between hole and electron bands (4), all in excellent agreement with the calculation. We also note the excellent agreement in the constant energy contours both above and below ε_F , as discussed above. In addition to this overall agreement between experiment and theory, we might ask if there is any direct signature of a Weyl semimetal that we can pinpoint from the experimental data alone²⁶. First, we consider a measurement of the Chern number, following the prescription discussed above for Type II Weyl cones. Formally, we can use the loop in Fig. 1(b) around either W_1 or W_2 to measure a Chern number of ± 1 ²⁶. Specifically, the topological Fermi arc will contribute one crossing, while the trivial surface state will contribute either zero crossings or two crossings of opposite Fermi velocity, with net contribution zero. However, in our experiment, the finite resolution prevents us from carrying out this counting. In particular, the linewidth of the surface state is comparable to its energy dispersion, so we cannot determine the sign of the Fermi velocity.

Next, we note that since the chiral charges of all Weyl point projections are ± 1 , we expect a disjoint arc connecting pairs of Weyl points, in one of two possible configurations, Figs. 4(e,f). From our calculation, we expect case Fig. 4(e). However, we observe no such disjoint arc in (3) in our spectrum. From calculation, we see

that this is perhaps reasonable because the Fermi arc is adjacent to trivial surface states, see the dotted lines in Figs. 4(c,d). Indeed, we can understand the Fermi arcs in Mo_xW_{1-x}Te₂ as arising from the large electron-like surface state (3) of Figs. 4(c,d), which we can imagine as being present whether or not there are Weyl points. Then, we can tune the system through a topological phase transition. Before the transition, the surface state is entirely trivial. After the transition, the Weyl point projections sit on (3) and “snip out” a topological Fermi arc from the large surface state. Formally, the Fermi arc terminates strictly on the Weyl points, while the remaining trivial surface states merge into the bulk in some generic way near the Weyl points. However, within any reasonable resolution, the topological and trivial surface states appear to connect at the Weyl points. As a result, we see no disjoint Fermi arc.

We might then ask if we can observe a kink, since the Fermi arc and the trivial surface state will generically meet at some angle. We note that we observe a kink in calculation, but not in the ARPES spectra presented here. We propose that a more complete pump-probe ARPES study of Mo_xW_{1-x}Te₂ may show such a kink. In particular, a full k_y dependence may catch a kink or “ripple” in the surface state, signaling a topological Fermi arc. If there is a difference in how well localized the Fermi arc is on the surface of the sample, compared to the trivial surface state, then a difference in the photoemission cross section may make one or the other feature brighter, allowing us to directly detect the arc. A composition de-

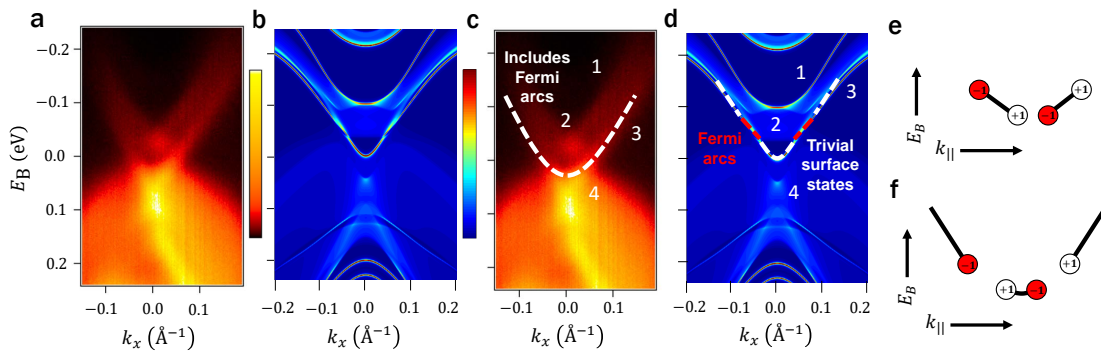


FIG. 4: **Signatures of Fermi arcs in $\text{Mo}_x\text{W}_{1-x}\text{Te}_2$.** (a) Pump-probe ARPES spectrum at $k_y = 0.225\text{\AA}^{-1}$. (b) *Ab initio* calculation at $k_y = k_{W1} = 0.215\text{\AA}^{-1}$, showing excellent overall agreement with the data. (c,d) Same as (a,b) but with key features in the data marked. (e,f) There are two possible scenarios for the connectivity of the arcs. The scenario in (e) is favored by our *ab initio* calculations. The surface state electron pocket (3) contains both the topological Fermi arcs and adjacent trivial surface states. While the Fermi arc is formally disconnected from the trivial surface states, in practice the trivial surface state merges into the bulk very close to the Weyl points, so that we do not observe a disjoint arc. Nonetheless, future measurements by pump-probe ARPES may allow us to observe a kink or “ripple” where the topological Fermi arc and trivial surface states meet, demonstrating that $\text{Mo}_x\text{W}_{1-x}\text{Te}_2$ is a Type II Weyl semimetal.

pendence may further show a systematic evolution of the kink, which would also prove an arc. Such an analysis is beyond the scope of this work. Here, we have shown theoretically that accessing the unoccupied band structure is crucial to show a Weyl semimetal in $\text{Mo}_x\text{W}_{1-x}\text{Te}_2$ and, in addition, we have directly accessed the unoccupied band structure in experiment and observed the surface state containing the topological Fermi arc. These results set the stage for directly demonstrating that $\text{Mo}_x\text{W}_{1-x}\text{Te}_2$ is a Type II Weyl semimetal.

Acknowledgements

I.B. and D.S. thank Moritz Hoesch and Timur Kim for support during synchrotron ARPES measurements at Beamline I05 of Diamond Lightsource in Didcot, UK. I.B. acknowledges the support of the US National Science Foundation GRFP. Y.I. is supported by the Japan Society for the Promotion of Science, KAKENHI 26800165. The ARPES measurements at Ames Lab were supported by the U.S. Department of Energy, Office of Science, Basic Energy Sciences, Materials Science and Engineer-

ing Division. Ames Laboratory is operated for the U.S. Department of Energy by Iowa State University under contract No. DE-AC02-07CH11358. M.N. is supported by start-up funds from the University of Central Florida. X.C.P., Y.S., B.G.W., G.H.W and F.Q.S. thank the National Key Projects for Basic Research of China (Grant Nos. 2013CB922100, 2011CB922103), the National Natural Science Foundation of China (Grant Nos. 91421109, 11522432, and 21571097) and the NSF of Jiangsu province (No. BK20130054). This work is also financially supported by the Singapore National Research Foundation (NRF) under NRF RF Award No. NRF-RF2013-08, the start-up funding from Nanyang Technological University (M4081137.070). T.-R.C. and H.-T.J. were supported by the National Science Council, Taiwan. H.-T.J. also thanks the National Center for High-Performance Computing, Computer and Information Network Center National Taiwan University, and National Center for Theoretical Sciences, Taiwan, for technical support. H.L. acknowledges the Singapore NRF under Award No. NRF-NRFF2013-03.

[†] Electronic address: ilyab@princeton.edu

[‡] Electronic address: z.liu@ntu.edu.sg

[§] Electronic address: songfengqi@nju.edu.cn

[¶] Electronic address: mzhasan@princeton.edu

¹ H. Weyl. *Elektron und Gravitation*. *Z. Phys.* **56** 330 (1929).

² M. Peskin & D. Schroeder. *An Introduction to Quantum Field Theory* (Perseus Books, Reading, MA, 1995)

³ Soluyanov, A. *et al.* Type II Weyl semimetals. *Nature* **527**, 495 (2015).

⁴ Grushin, A. G. Consequences of a condensed matter realization of Lorentz violating QED in Weyl semi-metals.

Phys. Rev. D **86** 045001 (2012).

⁵ Bergholtz, E. J. *et al.* Topology and Interactions in a Frustrated Slab: Tuning from Weyl Semimetals to $C > 1$ Fractional Chern Insulators. *Phys. Rev. Lett.* **114**, 016806 (2015).

⁶ Trescher, M. *et al.* Quantum transport in Dirac materials: Signatures of tilted and anisotropic Dirac and Weyl cones. *Phys. Rev. B* **91**, 115135 (2015).

⁷ Beenakker, C. Tipping the Weyl cone. *Journal Club for Condensed Matter Physics*, posted August, 2015.

⁸ Zyuzin, A. A. & Tiwari, R. P. Anomalous Hall

- Effect in Type-II Weyl Semimetals. Preprint at <http://arxiv.org/abs/1601.00890> (2016).
- ⁹ Isobe, H. & Nagaosa, N. Coulomb interaction effect in tilted Weyl fermion in two dimensions. *Phys. Rev. Lett.* **116**, 116803 (2016).
 - ¹⁰ T.-R. Chang *et al.* Arc-tunable Weyl fermion metallic state in $\text{Mo}_x\text{W}_{1-x}\text{Te}_2$. arXiv:1508.06723.
 - ¹¹ Y. Sun *et al.* Prediction of the Weyl semimetal in orthorhombic MoTe_2 . arXiv:1508.03501v2.
 - ¹² Z. J. Wang *et al.* MoTe_2 : Weyl and line node topological metal. arXiv:1511.07440v1.
 - ¹³ Chang, G. *et al.* A strongly robust Weyl fermion semimetal state in Ta_3S_2 . Preprint at <http://arxiv.org/abs/1512.08781> (2015).
 - ¹⁴ Koepernik, K. *et al.* TaIrTe_4 a ternary Type-II Weyl semi-metal. Preprint at <http://arxiv.org/abs/1603.04323> (2016).
 - ¹⁵ Autés, G. *et al.* Robust Type-II Weyl Semimetal Phase in Transition Metal Diphosphides XP_2 ($X = \text{Mo}, \text{W}$). Preprint at <http://arxiv.org/abs/1603.04624> (2016).
 - ¹⁶ L. Huang, T. M. McCormick, M. Ochi, Z. Zhao, M. Suzuki, R. Arita, Y. Wu, D. Mou, H. Cao, J. Yan, N. Trivedi, A. Kaminski. Spectroscopic evidence for type II Weyl semimetal state in MoTe_2 . arXiv:1603.06482.
 - ¹⁷ Y. Wu, N. H. Jo, D. Mou, L. Huang, S. L. Bud'ko, P. C. Canfield, A. Kaminski. Observation of Fermi Arcs in Type-II Weyl Semimetal Candidate WTe_2 . arXiv:1604.05176.
 - ¹⁸ C. Wang, Y. Zhang, J. Huang, S. Nie, G. Liu, A. Liang, Y. Zhang, B. Shen, J. Liu, C. Hu, Y. Ding, D. Liu, Y. Hu, S. He, L. Zhao, L. Yu, J. Hu, J. Wei, Z. Mao, Y. Shi, X. Jia, F. Zhang, S. Zhang, F. Yang, Z. Wang, Q. Peng, H. Weng, X. Dai, Z. Fang, Z. Xu, C. Chen, X. J. Zhou. Spectroscopic Evidence of Type II Weyl Semimetal State in WTe_2 . arXiv:1604.04218.
 - ¹⁹ K. Deng, G. Wan, P. Deng, K. Zhang, S. Ding, E. Wang, M. Yan, H. Huang, H. Zhang, Z. Xu, J. Denlinger, A. Fedorov, H. Yang, W. Duan, H. Yao, Y. Wu, S. Fan, H. Zhang, X. Chen, S. Zhou. Experimental observation of topological Fermi arcs in type-II Weyl semimetal MoTe_2 . arxiv:1603.08508.
 - ²⁰ J. Jiang, Z. K. Liu, Y. Sun, H. F. Yang, R. Rajamathi, Y. P. Qi, L. X. Yang, C. Chen, H. Peng, C.-C. Hwang, S. Z. Sun, S.-K. Mo, I. Vobornik, J. Fujii, S. S. P. Parkin, C. Felser, B. H. Yan, Y. L. Chen. Observation of the Type-II Weyl Semimetal Phase in MoTe_2 . arXiv:1604.00139.
 - ²¹ A. Liang, J. Huang, S. Nie, Y. Ding, Q. Gao, C. Hu, S. He, Y. Zhang, C. Wang, B. Shen, J. Liu, P. Ai, L. Yu, X. Sun, W. Zhao, S. Lv, D. Liu, C. Li, Y. Zhang, Y. Hu, Y. Xu, L. Zhao, G. Liu, Z. Mao, X. Jia, F. Zhang, S. Zhang, F. Yang, Z. Wang, Q. Peng, H. Weng, X. Dai, Z. Fang, Z. Xu, C. Chen, X. J. Zhou. Electronic Evidence for Type II Weyl Semimetal State in MoTe_2 , arXiv:1604.01706.
 - ²² N. Xu, Z. J. Wang, A. P. Weber, A. Magrez, P. Bugnon, H. Berger, C. E. Matt, J. Z. Ma, B. B. Fu, B. Q. Lv, N. C. Plumb, M. Radovic, E. Pomjakushina, K. Conder, T. Qian, J. H. Dil, J. Mesot, H. Ding, M. Shi. Discovery of Weyl semimetal state violating Lorentz invariance in MoTe_2 , arXiv:1604.02116.
 - ²³ F. Y. Bruno, A. Tamai, Q. S. Wu, I. Cucchi, C. Barreteau, A. de la Torre, S. McKeown Walker, S. Ricc, Z. Wang, T. K. Kim, M. Hoesch, M. Shi, N. C. Plumb, E. Giannini, A. A. Soluyanov, F. Baumberger. Surface states and bulk electronic structure in the candidate type-II Weyl semimetal WTe_2 . arXiv:1604.02411.
 - ²⁴ Xu, S.-Y. *et al.* Discovery of Lorentz-violating Weyl fermion semimetal state in LaAlGe materials. arXiv:1603.07318.
 - ²⁵ Chang, G. *et al.* Theoretical prediction of magnetic and noncentrosymmetric Weyl fermion semimetal states in the $R\text{-Al-X}$ family of compounds ($R = \text{rare Earth}$, $\text{Al} = \text{aluminium}$, $X = \text{Si, Ge}$). arXiv:1604.02124.
 - ²⁶ Belopolski, I. *et al.* Criteria for Directly Detecting Topological Fermi Arcs in Weyl Semimetals. *Phys. Rev. Lett.* **116**, 066802 (2016).
 - ²⁷ See the Supplemental Material for additional ARPES data on the electronic structure of $\text{Mo}_x\text{W}_{1-x}\text{Te}_2$ and the methods.
 - ²⁸ T. M. McCormik, I. Kimchi & N. Trivedi. Minimal models for topological Weyl semimetals. arXiv:1604.03096.
 - ²⁹ Y. Ishida *et al.* Time-resolved photoemission apparatus achieving sub-20-meV energy resolution and high stability. *Rev. Sci. Instr.* **85**, 123904 (2014).
 - ³⁰ B. E. Brown. The crystal structures of WTe_2 and high-temperature MoTe_2 . *Acta. Cryst.* **20** 268 (1966).
 - ³¹ R. Jiang *et al.* Tunable vacuum ultraviolet laser based spectrometer for angle-resolved photoemission spectroscopy. *Rev. Sci. Instr.* **85**, 033902 (2014).
 - ³² G. M. Sheldrick. *SADABS* (University of Göttingen, Göttingen, Germany, 1996).
 - ³³ *CrystalClear, v1.3.5* (Rigaku Corp., The Woodlands, TX, 1999).
 - ³⁴ G. M Sheldrick. *SHELXTL, v5.1* (Bruker-AXS, Madison, WI, 1998).
 - ³⁵ P. E. Blöchl. Projector augmented-wave method. *Phys. Rev. B.* **50**, 17953 (1994).
 - ³⁶ G. Kresse & J. Joubert. From ultrasoft pseudopotentials to the projector augmented-wave method. *Phys. Rev. B.* **59**, 1758 (1999).
 - ³⁷ G. Kresse & J. Hafner. *Ab initio* molecular dynamics for open-shell transition metals. *Phys. Rev. B.* **48**, 13115 (1993).
 - ³⁸ G. Kresse & J. Furthmüller. Efficiency of *ab initio* total energy calculations for metals and semiconductors using a plane-wave basis set. *Comput. Mater. Sci.* **6**, 15 (1996).
 - ³⁹ G. Kresse & J. Furthmüller. Efficient iterative schemes for *ab initio* total energy calculations using a plane-wave basis set. *Phys. Rev. B.* **54**, 11169 (1996).
 - ⁴⁰ J. P. Perdew, K. Burke & M. Ernzerhof. Generalized gradient approximation made simple. *Phys. Rev. Lett.* **77**, 3865 (1996).
 - ⁴¹ N. Marzari & D. Vanderbilt. Maximally localized generalized Wannier functions for composite energy bands. *Phys. Rev. B* **56**, 12847 (1997).
 - ⁴² I. Souza, N. Marzari & D. Vanderbilt. Maximally localized Wannier functions for entangled energy bands. *Phys. Rev. B* **65**, 035109 (2001).
 - ⁴³ A. A. Mostofi *et al.* Wannier90: a tool for obtaining maximally-localized Wannier functions. *Comp. Phys. Commun.* **178**, 685 (2008).
 - ⁴⁴ C. Franchini *et al.* Maximally localized Wannier functions in LaMnO_3 within PBE+U, hybrid functionals and partially self-consistent GW: an efficient route to construct *ab initio* tight-binding parameters for e_g perovskites. *J. Phys. Cond. Mat.* **24**, 235602 (2012).
 - ⁴⁵ H. J. Zhang *et al.* Topological insulators in Bi_2Se_3 , Bi_2Te_3 and Sb_2Te_3 with a single Dirac cone on the surface. *Nat. Phys.* **5**, 438 (2009).